Journal of Sound and Vibration 337 (2015) 181–198

Contents lists available at ScienceDirect

Journal of Sound and Vibration

journal homepage: www.elsevier.com/locate/jsvi

A "Pseudo-excitation" approach for structural damage identification: From "Strong" to "Weak" modality

Hao Xu[a,b], Zhongqing Su[a,b,*], Li Cheng[a,b], Jean-Louis Guyader[c]

[a] The Hong Kong Polytechnic University Shenzhen Research Institute, Shenzhen 518057, PR China
[b] The Department of Mechanical Engineering, The Hong Kong Polytechnic University, Kowloon, Hong Kong Special Administrative Region
[c] Laboratoire Vibrations Acoustique, Institut National des Sciences Appliquées (INSA) de Lyon, 69621, Villeurbanne, France

ARTICLE INFO

Article history:
Received 9 July 2014
Received in revised form
16 September 2014
Accepted 21 October 2014
Handling Editor: I. Trendafilova
Available online 18 November 2014

ABSTRACT

A damage characterization framework based on the "pseudo-excitation" (PE) approach has recently been established, aimed at quantitatively identifying damage in beam-, plate-, and shell-like structural components. However, it is envisaged that the effectiveness of the PE approach can be restricted in practical implementation, due to the involvement of high-order derivatives of structural dynamic deflections, in which measurement noise and uncertainties can overwhelm the damage-associated signal features upon mathematical differentiation. In this study, the PE approach was revamped by introducing the weighted integration, whereby the prerequisite of satisfying the local equilibrium conditions was relaxed from "point-by-point" to "region-by-region". The revamped modality was thus colloquially referred to as "weak formulation" of the PE approach, as opposed to its original version which is contrastively termed as "strong formulation". By properly configuring a weight function, noise immunity of the PE approach was enhanced, giving rise to improved detection accuracy and precision even under noisy measurement conditions. Furthermore, the 'weak formulation' was extended to a series of coherent variants through partial integration, rendering a multitude of detection strategies by selecting measurement parameters and configurations. This endowed the PE approach with flexibility in experimental manipulability, so as to accommodate various detection requirements. As an application of the "weak formulation", a continuous gauss smoothing (CGS)-based detection scheme was developed, and validated by localizing multiple cracks in a beam structure, showing fairly improved noise tolerance.

1. Introduction

"Pseudo-excitation" (PE) is a damage detection framework, recently developed by virtue of exploring and calibrating damage-induced perturbation to the local dynamic equilibrium of a structural component [1–4]. The effectiveness of the approach has been examined rigorously, using various damage scenarios in diverse structural components (e.g., beam [1,2], and plate [3]) as well as complex engineering structures (e.g., multi-component structures [3], and steel-reinforced concrete slabs [4]). Notably, the PE approach is not restricted by the type of damage (viz., crack, notch, delamination, material

* Corresponding author at: The Department of Mechanical Engineering, The Hong Kong Polytechnic University, Kowloon, Hong Kong Special Administrative Region. Tel.: +852 2766 7818.

http://dx.doi.org/10.1016/j.jsv.2014.10.035
0022-460X/

Nomenclature

c [m]	Standard deviation of gauss function
D [Nm]	Bending stiffness of thin plate
DI	Damage index of 'strong formulation' of PE technique
$\overline{\mathrm{DI}}$	Damage index of 'weak formulation' of PE technique
d_m [m]	Distance between adjacent measurement points
f [Hz]	Vibration frequency
h [m]	Thickness of plate
I [m^4]	Moment of inertia
N	Number of points in the integration interval
S [m^2]	Cross section area
x_c [m]	Center of integration interval

degradation, etc.) and its number within the inspection region, and the approach has proven sensitivity to the boundary of a damaged zone in particular. Residing on an explicit physical cornerstone, the PE approach can be used to construct assorted damage indices (DIs) with different structural vibration parameters. It exhibits prominent advantages in some aspects over conventional global vibration-based [5–11] or local guided-wave-based [12–19] damage detection techniques, including the following:

(1) higher sensitivity to damage of small dimension, owing to the use of high-order equation of motion (in contrast, a global vibration-based approach is usually insensitive to damage before it reaches a conspicuous extent, while a local guided-wave-based method can be limited by the wavelength of the selected wave mode);
(2) capability of locally interrogating the inspection region point-by-point, thus independent of a global model of the entire structure;
(3) by the same token, applicability to detection of multi-damage, regardless of the type of respective damage;
(4) independence of prior information on structural boundaries (meaning the complexity of a system would not limit the applicability of the approach) and modal behavior (i.e., a deliberately generated mode shape of the structure is not of necessity); and
(5) no need to reference a benchmark structure or a baseline signal, therefore immunity from possible interferences from fluctuating environment (e.g., varying temperature).

The original version of the PE approach requests that the local equilibrium of the structural component be examined rigorously at every single inspection point. Such a 'strong' prerequisite may downgrade practicability of the PE approach, as a result of the connatural vulnerability of the constructed DI to measurement noise and uncertainties. That is because the local dynamic equilibrium of a structural component features high-order derivatives of the structural dynamic deflection (e.g., $\mathrm{d}^4v(x)/\mathrm{d}x^4$ for a beam component where $v(x)$ is the flexural displacement of the component at location x, while $\partial^4 v(x,y)/\partial x^4$ for a plate component with $v(x,y)$ is the flexural displacement of the component at (x,y)). During the fourth-order differentiation, measurement noise and uncertainties unavoidably included in $v(x)$ and $v(x,y)$ are to be magnified to a significant level, masking the damage-induced changes in DI and jeopardizing the robustness of the approach.

In recognition of such deficiencies, the original PE approach was revamped by introducing the weighted integration, aimed at enhancing the noise immunity of the approach when deployed under noisy measurement conditions. In brief, the prerequisite of satisfying the local equilibrium is relaxed from "point-by-point" to "region-by-region". To highlight such relaxation, the revamped modality of the PE approach is colloquially called "weak formulation", as opposed to its original version otherwise termed as "strong formulation". Such relaxation creates a twofold merit:

(1) by properly configuring a weight function, the effect of measurement noise and uncertainties strengthened upon high-order differentiation can be largely reduced within a selected integration interval; and
(2) by properly selecting measurement parameters and configurations, a series of coherent variants of the "weak formulation" can be derived using partial integration, leading to a multitude of detection strategies, to accommodate various detection requirements.

As an application, a weighted function was designed using the classic Gaussian function, and the correspondingly developed "weak formulation", called *continuous gauss smoothing* (CGS), was validated by localizing multiple cracks in a beam-like structure.

2. "Strong formulation" of PE approach

Considering an intact Euler–Bernoulli beam component with a homogeneous isotropic material nature, a one-dimensional DI, denoted by $\mathrm{DI}(x,t)$, can be defined by quantifying damage-induced local perturbation to the dynamic equilibrium of the component, which reads as

$$\mathrm{DI}(x,t)=\frac{\partial^2}{\partial x^2}\left[EI(x)\frac{\partial^2 v(x,t)}{\partial x^2}\right]+\rho S(x)\frac{\partial^2 v(x,t)}{\partial t^2}, \tag{1a}$$

where $v(x,t)$ is the dynamic deflection of the component at location x at time t. E, ρ, I and S are the complex modulus of elasticity (comprehending material damping), density, cross-sectional moment of inertia, and area of the component in its pristine status, respectively. It is noteworthy that $v(x,t)$ can be obtained from a broad spectrum of vibration conditions of the structure that are either instantaneous or steady. For a pristine beam component (free of any damage in the absence of external surface excitation), $\mathrm{DI}(x,t)=0$. As Eq. (1a) describes a local equilibrium, the boundary conditions of the beam are not of interest.

Specifically, under a steady vibration, $v(x,t)$ can be replaced with the steady vibration deflection of the beam, $w(x)$. Assuming that the beam possesses a uniform cross-section and constant material properties, Eq. (1a) can be simplified, in a harmonic regime, as

$$\mathrm{DI}(x)=EI\frac{\mathrm{d}^4w(x)}{\mathrm{d}x^4}-\rho S\omega^2w(x), \tag{1b}$$

where ω is the angular vibration frequency of the steady vibration. In the case that the excitation is not harmonic, one frequency component in the frequency domain after Fourier transform can also be used.

Eqs. (1a) and (1b) reveal that the PE approach is, in essence, a dynamic response-based damage detection philosophy. In practice, $w(x)$ can be measured discretely using well-defined techniques such as accelerometers, laser holography or Doppler laser vibrometer, with which DI can be constructed via a finite difference scheme. By way of illustration, DI at measurement point i in a discrete form can be expressed, by involving four neighboring measurement points from point $i-2$ to $i+2$, as

$$\mathrm{DI}_i=\frac{EI}{d_m^4}(w_{i-2}-4w_{i-1}+6w_i-4w_{i+1}+w_{i+2})-\rho S\omega^2w_i, \tag{1c}$$

where d_m is the distance between two adjacent measurement points and w_i is the flexural displacement measured at point i.

Similarly, a two-dimensional DI can be derived for a homogeneous isotropic plate-like component, based on the plate theory, as

$$\mathrm{DI}(x,y,t)=D\nabla^4v(x,y,t)+\rho h\frac{\partial^2v(x,y,t)}{\partial t^2}, \tag{2a}$$

or, under a steady vibration, as

$$\mathrm{DI}(x,y)=D\nabla^4w(x,y)+\rho h\omega^2w(x,y), \tag{2b}$$

where $D=Eh^3/12(1-\nu^2)$. In the above, $v(x,y,t)$ and $w(x,y)$ signify the dynamic deflection and vibration deflection under steady vibration, respectively; D is the bending stiffness; h and ν are the thickness and Poisson's ratio of the component, respectively.

Likewise, the two-dimensional DI can be re-defined in a discrete form, using a finite difference scheme, as

$$\mathrm{DI}_{i,j}=D_c\left(\chi_{i,j}^{4x}+2\chi_{i,j}^{2x2y}+\chi_{i,j}^{4y}\right)+ph_c\omega^2w_{i,j}. \tag{2c}$$

Here $w_{i,j}$ is the flexural displacement of the plate measured at point (i,j), and

$$\chi_{i,j}^{4x}=\frac{\partial^4w}{\partial x^4}=\frac{1}{\Delta_x^4}(w_{i+2,j}-4w_{i+1,j}+6w_{i,j}-4w_{i-1,j}+w_{i-2,j}), \tag{2d}$$

$$\chi_{i,j}^{4y}=\frac{\partial^4w}{\partial y^4}=\frac{1}{\Delta_y^4}(w_{i,j+2}-4w_{i,j+1}+6w_{i,j}-4w_{i,j-1}+w_{i,j-2}), \tag{2e}$$

$$\chi_{i,j}^{2x2y}=\frac{\partial^4w}{\partial^2x\partial^2y}=\frac{1}{\Delta_x^2\Delta_y^2}(w_{i+1,j+1}-2w_{i+1,j}+w_{i+1,j-1}-2w_{i,j+1}+4w_{i,j}-2w_{i,j-1}+w_{i-1,j-1}-2w_{i-1,j+1}w_{i-1,j-1}), \tag{2f}$$

where Δ_x and Δ_y are the intervals between two adjacent measurement points along the x- and y-axes, respectively.

The underlying philosophy of PE approach-based damage identification can be stated as follows:

(1) for a pristine component in its intact status and in the absence of any external excitation, the DI (defined by Eqs. (1) or (2)) remains zero across the component, owing to the strict satisfaction of local equilibrium on every infinitesimal fragment of the component. By way of illustration, an Euler–Bernoulli beam fragment is shown schematically in Fig. 1(a). In the figure, $M(x,t)$ and $Q(x,t)$ are the internal bending moment and shear force, respectively; $q(x,t)$ is the distribution density of the external excitation, with $q(x,t)=0$ signifying the absence of any external excitation; and

(2) when damage (say a damaged zone Ω) occurs, DI along the boundary of Ω fluctuates due to the damage-induced shear forces, bending and torsion moments; within Ω, DI smoothly varies, provided the material and geometry are continuous within Ω (but they can be different from those outside of Ω). Note that, although the isolated fragment in Fig. 1(a) is free of any external force, the internal forces and moments exerted by the rest of the component still exist, on the sharing boundaries between the fragment and the rest of the component.

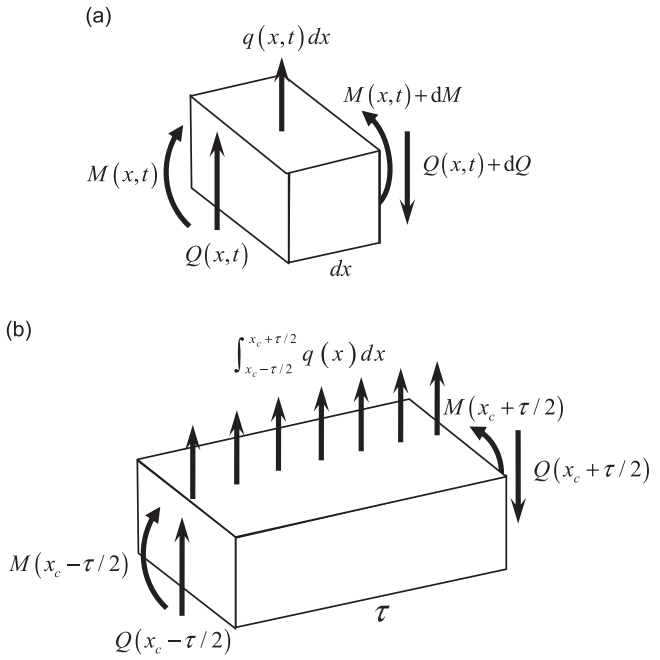

Fig. 1. Forces and moments, satisfying local equilibrium, applied on (a) an infinitesimal beam element and (b) a beam fragment with finite length.

The nature of the DI alludes to that the vibration of a structural component bearing a damaged zone Ω can be equivalent to that of its pristine counterpart, with fictitious "*external*" forces applied on the surface over Ω. Therefore, these fictitious "*external*" forces are referred to as "*pseudo-excitation*" (PE). Equations (1) and (2) also articulate that DI, though associated with the damage, is developed using the material and geometrical parameters of the component in an intact region (free of damage). Any drastic oscillation in DI implies the existence of damage therein; and the distribution profile of DI can thus be used to quantitatively evaluate a damaged zone. It has been demonstrated that the most prominent oscillations of DI can be perceived along the boundaries of a damaged zone [1].

3. "Weak Formulation" of PE approach

3.1. Motivation

However, the DI based on the "strong formulation" of the PE approach is prone to the contamination from measurement noise and uncertainties which may overwhelm the damage-induced perturbation to the local equilibrium. That is because the noise and uncertainties contained in an experimentally captured $w(x)$ (for beam component) or $w(x,y)$ (for plate component) can become overwhelmingly dominant upon fourth-order differentiation (e.g., $\partial^4 w(x)/\partial x^4$ or $\partial^4 w(x,y)/\partial x^4$).

For illustration, the distribution of DI constructed via numerical simulation for a plate component is presented in Fig. 2(a) and (b), respectively, for the noise-free and noise-corrupted measurement [3] (denoted by $\mathrm{DI}_{i,j}^{\mathrm{exact}}$ and $\mathrm{DI}_{i,j}^{\mathrm{noisy}}$, respectively). In the absence of noise, Fig. 2(a), the damaged zone, small in size, can be located precisely using the PE approach, as evidenced by the prominent changes in DI along the damaged zone, contrasting the poor detection resolution obtained using the noise-contaminated vibration displacements as shown in Fig. 2(b). It is noteworthy that the level of the added noise, in Fig. 2(b), is as low as only 1 percent of the magnitude of the maximum vibration displacement of the plate. The unintelligible detection results from $\mathrm{DI}_{i,j}^{\mathrm{noisy}}$ can be attributed to the strong noisy interference in the damage-induced changes in DI after fourth-order derivation of the vibration displacements. It is thus of vital necessity to enhance the noise immunity of the PE approach.

3.2. General expression of "Weak Formulation"

For the Euler–Bernoulli beam component in Fig. 1(a), the DI constructed using Eq. (1b)– the "strong formulation" of the PE approach – can be retrofitted within an integration interval, instead of at every single point, by introducing the weighted integration as

$$\overline{\mathrm{DI}} = \int_{x_c-\tau/2}^{x_c+\tau/2} [\mathrm{DI}(x)\cdot\eta(x-x_c)]\mathrm{d}x, \tag{3}$$

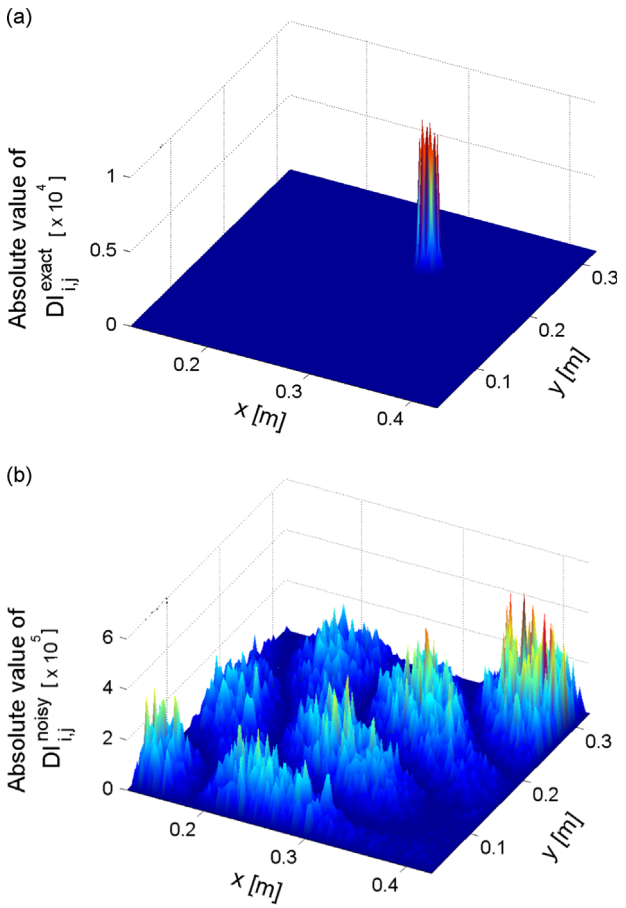

Fig. 2. Two-dimensional DI constructed for plate components using vibration displacements (a) with and (b) without noise influence.

where $\overline{\mathrm{DI}}$ is the re-defined DI within integration interval $[x_c-\tau/2,\ x_c+\tau/2]$, centralized at x_c with a length of τ. This integration interval is denoted by Ξ in what follows. $\eta(x)$ is a weighting function which can, in principle, take an arbitrary form. The bar over DI signifies the re-defined DI is an integral within Ξ rather than at a specific point. By regulating x_c and τ, the position and length of Ξ can be adjusted, serving as a "scanning window" to examine the entire component 'region-by-region.' Similarly, the two-dimensional expression of $\overline{\mathrm{DI}}$ towards a plate component can also be developed using the dual-integration along $x-$ and $y-$axes with a two-dimensional integration interval.

Fluctuation of $\overline{\mathrm{DI}}$ can be an indicator to damage occurrence during the "scanning" of the window. Different from the detection using DI (with "strong formulation") to examine the inspection region "point-by-point", the detection based on the use of $\overline{\mathrm{DI}}$ is executed "region-by-region". In that sense, the prerequisite of satisfying the local equilibrium condition has been relaxed from "point-by-point" to "region-by-region".

In an extreme case by setting $\eta(x)=1$, it has $\overline{\mathrm{DI}}=\int_{\Xi}\mathrm{DI}(x)\mathrm{d}x$, which possesses explicit physical implication: as shown in Fig. 1(b) for the exemplary fragment in Fig. 1(a), $\overline{\mathrm{DI}}$ represents the summation of all the "pseudo-exactions" applied over the surface of Ξ. Certainly, $\eta(x)$ can be designed optimally, by taking a sophisticated form so as to accommodate specific purposes and to improve the detection accuracy (to be detailed in subsequent sections).

3.3. Variants of "Weak Formulation"

Substituting Eq. (1b) into (3) yields

$$\overline{\mathrm{DI}}_4=\int_{\Xi}\left[EI\frac{\mathrm{d}^4w(x)}{\mathrm{d}x^4}-\rho S\omega^2w(x)\right]\eta(x-x_c)\mathrm{d}x. \tag{4a}$$

The subscript "4" accentuates that this damage index is based on the fourth-order derivative of $w(x)$. To take a step further, Eq. (4a) can be extended to the following variants, using partial integration, as

$$\overline{\mathrm{DI}}_3 = EI\left[\frac{\mathrm{d}^3 w(x)}{\mathrm{d}x^3}\cdot\eta(x-x_c)\right]_{x_c-\tau/2}^{x_c+\tau/2} - \int_{\Xi}\left[EI\frac{\mathrm{d}^3 w(x)}{\mathrm{d}x^3}\cdot\frac{\mathrm{d}\eta(x-x_c)}{\mathrm{d}x} + \rho S\omega^2\cdot\eta(x-x_c)\cdot w(x)\right]\mathrm{d}x, \tag{4b}$$

$$\overline{\mathrm{DI}}_2 = EI\left[\frac{\mathrm{d}^3 w(x)}{\mathrm{d}x^3}\cdot\eta(x-x_c) - \frac{\mathrm{d}^2 w(x)}{\mathrm{d}x^2}\cdot\frac{\mathrm{d}\eta(x-x_c)}{\mathrm{d}x}\right]_{x_c-\tau/2}^{x_c+\tau/2} + \int_{\Xi}\left[EI\frac{\mathrm{d}^2 w(x)}{\mathrm{d}x^2}\cdot\frac{\mathrm{d}^2\eta(x-x_c)}{\mathrm{d}x^2} - \rho S\omega^2\cdot\eta(x-x_c)\cdot w(x)\right]\mathrm{d}x, \tag{4c}$$

$$\begin{aligned}\overline{\mathrm{DI}}_1 = EI&\left[\frac{\mathrm{d}^3 w(x)}{\mathrm{d}x^3}\cdot\eta(x-x_c) - \frac{\mathrm{d}^2 w(x)}{\mathrm{d}x^2}\cdot\frac{\mathrm{d}\eta(x-x_c)}{\mathrm{d}x} + \frac{\mathrm{d}w(x)}{\mathrm{d}x}\cdot\frac{\mathrm{d}^2\eta(x-x_c)}{\mathrm{d}x^2}\right]_{x_c-\tau/2}^{x_c+\tau/2}\\ &- \int_{\Xi}\left[EI\frac{\mathrm{d}w(x)}{\mathrm{d}x}\cdot\frac{\mathrm{d}^3\eta(x-x_c)}{\mathrm{d}x^3} + \rho S\omega^2\cdot\eta(x-x_c)\cdot w(x)\right]\mathrm{d}x,\end{aligned} \tag{4d}$$

and

$$\begin{aligned}\overline{\mathrm{DI}}_0 = EI&\left[\frac{\mathrm{d}^3 w(x)}{\mathrm{d}x^3}\cdot\eta(x-x_c) - \frac{\mathrm{d}^2 w(x)}{\mathrm{d}x^2}\cdot\frac{\mathrm{d}\eta(x-x_c)}{\mathrm{d}x} + \frac{\mathrm{d}w(x)}{\mathrm{d}x}\cdot\frac{\mathrm{d}^2\eta(x-x_c)}{\mathrm{d}x^2} - w(x)\cdot\frac{\mathrm{d}^3\eta(x-x_c)}{\mathrm{d}x^3}\right]_{x_c-\tau/2}^{x_c+\tau/2}\\ &+ \int_{\Xi}\left[EI\frac{\mathrm{d}^4\eta(x-x_c)}{\mathrm{d}x^4} - \rho S\omega^2\cdot\eta(x-x_c)\right]w(x)\mathrm{d}x.\end{aligned} \tag{4e}$$

In the above, the subscript of $\overline{\mathrm{DI}}_k$ ($k=0,\ 1,\ 2,\ 3,\ 4$) points out the highest order of $w(x)$ involved. $\overline{\mathrm{DI}}_k$ defined by Eqs. (4b) to (4e) are the variants of original "weak formulation" (Eq. (4a)).

The "weak formulation" defined by Eq. (4a), as well as its variants in different modalities (from Eqs. (4b) to (4e)), features a twofold characteristic:

(1) mathematically, $\overline{\mathrm{DI}}_k$ of different orders ($k=0,\ 1,\ 2,\ 3,\ 4$) are identical, independent of $\eta(x)$, although numerical errors might exist among different expressions in numerical computation; and
(2) any variant of "weak formulation" contains two terms: an "integration part" ($\int_{\Xi}[\,]\mathrm{d}x$) – the operation of integration within Ξ, and a "boundary part" ($-[\,]_{x_c-\tau/2}^{x_c+\tau/2}$) – the operation of subtracting relevant terms at the boundary of Ξ. Specifically, in the "integration part", the order of derivative of $w(x)$ decreases stepwise from three in $\overline{\mathrm{DI}}_3$ to zero in $\overline{\mathrm{DI}}_0$; while in the "boundary part", the order of derivative of $\eta(x)$ increases from zero in $\overline{\mathrm{DI}}_3$ to three in $\overline{\mathrm{DI}}_0$.

The above characteristic endows the "weak formulation" with a dual-merit, compared with its strong counterpart:

(1) an enhanced immunity to noise interference, because the level of measurement noise can be largely averaged due to the weighted integration; and
(2) a diversity of experimental implementation options by using the variants of $\overline{\mathrm{DI}}_k$. This offers certain flexibility towards practical applications of the PE approach, as elaborated in the following

3.3.1. ***Flexible selection of*** $\eta(x)$

The variants, compared with their original form of the 'weak formulation,' take a more complicated appearance which involves more parameters and in particular at a lower differential order. It is however feasible to simplify the expression of these variants by tactically choosing $\eta(x)$. A sophisticated design of $\eta(x)$ is able to achieve a twofold aim: (i) suppressing the influence from measurement noise and strengthening signal features pertaining to damage, and (ii) eliminating several terms in the variants which may be difficult to obtain, for instance, the "integration part" or "boundary part", to simplify the expression of $\overline{\mathrm{DI}}_k$.

3.3.2. *Flexible selection of measurands*

The derivatives of $w(x)$ in the variants are linked to different measurands to be acquired. For instance, $\mathrm{d}^2 w(x)/\mathrm{d}x^2$ and $\mathrm{d}w(x)/\mathrm{d}x$ can be obtained by measuring the local strains and angle of rotation of the component, respectively. Thus, various measurands can be chosen depending on the needs and available measurement means, for example, to achieve an enhanced noise immunity by measuring multiple types of measurands.

3.3.3. *Flexible selection of measurement points*

The "integration part" and "boundary part" are mutually independent in the variants, and this creates the possibility to construct two parts separately – using different densities of measurement points – for example a higher density of measurement points within the "integration part", while lower in the "boundary part". Notably, a sophisticated adjustment

of measurement density and positions can facilitate optimization of the experimental configuration, in turn leading to improved detection accuracy (to be discussed in later sections).

3.3.4. Flexible selection of noise-influenced terms

It is apparent that the measurement noise and uncertainties are included in $w(x)$ and its derivatives only. From $\overline{\mathrm{DI}}_4$ to $\overline{\mathrm{DI}}_0$, the noise-influenced terms are transferred among the derivative of $w(x)$ with various orders. Particularly, as seen in $\overline{\mathrm{DI}}_0$, the measurement noise is associated with $w(x)$ in the "integration part" only, while all the high-order derivatives of $w(x)$, including measurement noise and uncertainties, are transferred to the "boundary part". Such a trait of the "weak formulation" can be conducive to minimizing the noise influence on detection precision under noisy measurement conditions, by properly selecting the measurement parameters (to be discussed in subsequent sections).

From the above statements, it can be seen that if using Eq. (4a) only, the "weak formulation" shows large similarity with other signal processing techniques such as wavelet transform, the principle of which also resides on the weighted integration. However, the variants of the "weak formulation" play a number of important roles far beyond signal processing, largely contributing to the development of new detection strategies.

4. Implementation of "Weak Formulation"

It is straightforward that the selection of $\eta(x)$ essentially determines the ultimate form of $\overline{\mathrm{DI}}_k$. By way of illustration, a classic Gaussian function is used as $\eta(x)$, to configure the "weak formulation".

4.1. Principle

With the classic Gaussian function, $\eta(x)$ can be defined as

$$\eta(x) = e^{-(x^2/2c^2)}, \quad x \in [-\tau/2, \tau/2] \tag{5}$$

where c is the standard deviation of the Gaussian function. The mathematical property of the Gaussian function [20] confines majority of the energy of $\eta(x)$ within Ξ, while vanishing at boundaries of Ξ, as explained in Fig. 3(a). Furthermore, the derivatives of $\eta(x)$ at different orders, from $\mathrm{d}\eta(x)/\mathrm{d}x$ to $\mathrm{d}^4\eta(x)/\mathrm{d}x^4$, as well as at the boundaries, become zero, as illustrated in Fig. 3(b) to (e). This characteristic of the Gaussian function eliminates all the "boundary parts" in the variants of "weak formulation" in Eqs. (4b)–(4e), greatly simplifying the expression of $\overline{\mathrm{DI}}_k$. Benefiting from this, the accordingly simplified "weak formulation" and its variants at different orders, termed as *continuous gauss smoothing* (CGS), read as

$$\overline{\mathrm{DI}}_{4-CGS} = \int_{x_c-\tau/2}^{x_c+\tau/2} \left[EI\frac{\mathrm{d}^4 w(x)}{\mathrm{d}x^4} - \rho S\omega^2 w(x) \right] \eta(x-x_c)\mathrm{d}x, \tag{6a}$$

$$\overline{\mathrm{DI}}_{3-CGS} = -\int_{x_c-\tau/2}^{x_c+\tau/2} \left[EI\frac{\mathrm{d}^3 w(x)}{\mathrm{d}x^3} \cdot \frac{\mathrm{d}\eta(x-x_c)}{\mathrm{d}x} + \rho S\omega^2 \cdot \eta(x-x_c) \cdot w(x) \right] \mathrm{d}x, \tag{6b}$$

$$\overline{\mathrm{DI}}_{2-CGS} = \int_{x_c-\tau/2}^{x_c+\tau/2} \left[EI\frac{\mathrm{d}^2 w(x)}{\mathrm{d}x^2} \cdot \frac{\mathrm{d}^2\eta(x-x_c)}{\mathrm{d}x^2} - \rho S\omega^2 \cdot \eta(x-x_c) \cdot w(x) \right] \mathrm{d}x, \tag{6c}$$

$$\overline{\mathrm{DI}}_{1-CGS} = -\int_{x_c-\tau/2}^{x_c+\tau/2} \left[EI\frac{\mathrm{d}w(x)}{\mathrm{d}x} \cdot \frac{\mathrm{d}^3\eta(x-x_c)}{\mathrm{d}x^3} + \rho S\omega^2 \cdot \eta(x-x_c) \cdot w(x) \right] \mathrm{d}x, \tag{6d}$$

$$\overline{\mathrm{DI}}_{0-CGS} = \int_{x_c-\tau/2}^{x_c+\tau/2} \left[EI\frac{\mathrm{d}^4\eta(x-x_c)}{\mathrm{d}x^4} - \rho S\omega^2 \cdot \eta(x-x_c) \right] w(x)\mathrm{d}x. \tag{6e}$$

"CGS" in the subscript differentiates the simplified "weak formulation" from its original forms defined by Eq. (4). By changing Ξ (via adjusting x_c in Eq. (6)) within which $\eta(x)$ is defined, the integration window can shift along the inspection region.

4.2. Numerical simulation

The feasibility of using CGS for quantitative identification of structural damage was evaluated using the finite element (FE) simulation first.

4.2.1. FE model

Considering an Euler–Bernoulli cantilever beam, 1200 mm in length, with geometrical and material properties listed in Table 1, the beam was clamped at its left end as shown in Fig. 4.

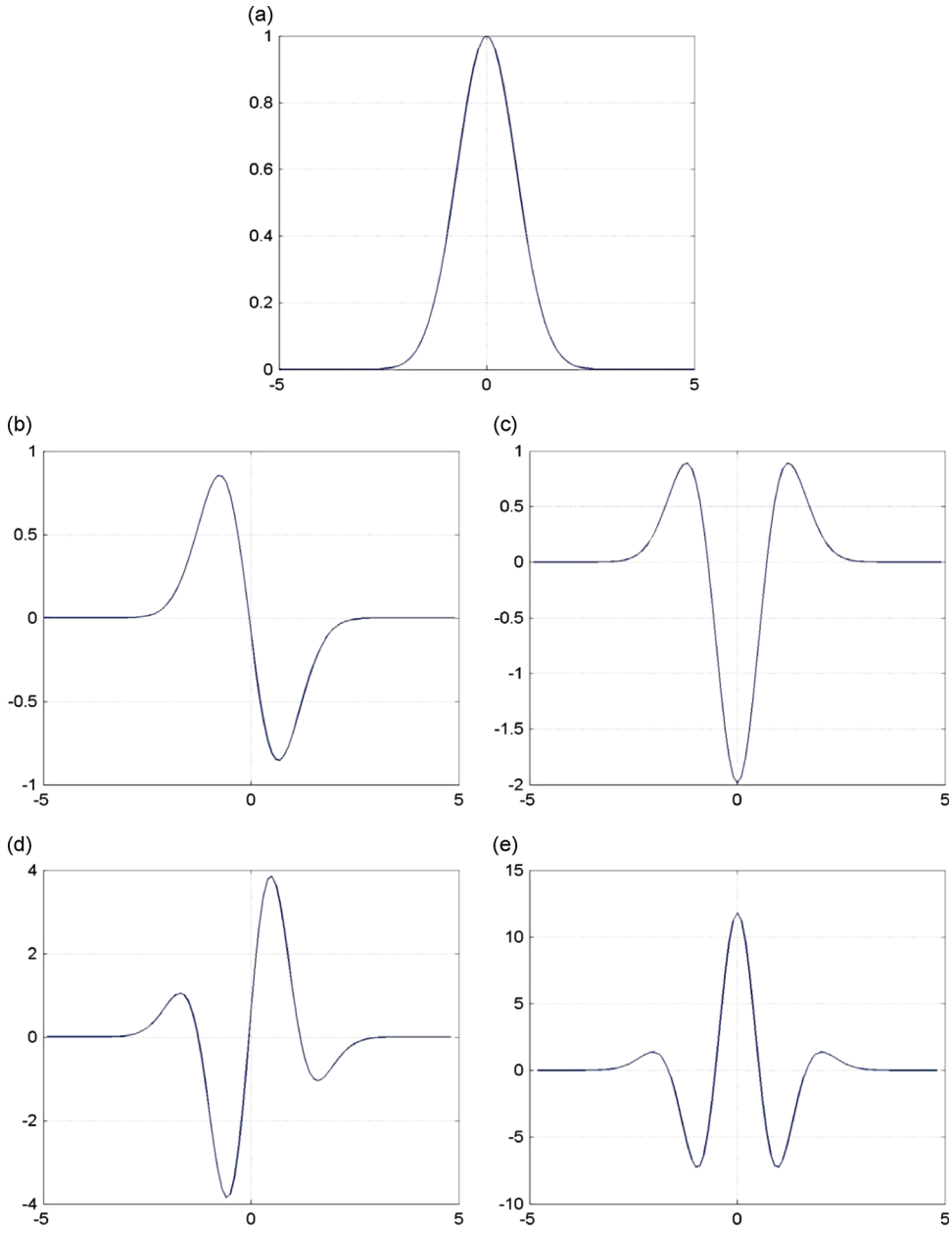

Fig. 3. The characteristic profiles of (a) $\eta(x)$; (b) $d\eta(x)/dx$; (c)$d^2\eta(x)/dx^2$; (d) $d^3\eta(x)/dx^3$; and (e) $d^4\eta(x)/dx^4$ ($\tau = 10$).

An FE model for the beam, with 600 beam elements evenly across the beam length, was created using commercial FE code ANSYS®. A harmonic point-force excitation of 1000 Hz was applied at $x = 10$ mm (referring to Fig. 4 for the coordinate system). Note that selecting a resonance frequency of the structure is not of necessity; actually it is preferable to apply this method at an off-resonance regime, so as to minimize the effect of system damping. But it has been shown in a previous study [1] that a relatively high frequency corresponds to strong noise immunity of the PE technique, and thus the frequency was selected to be higher than the third natural frequency. The beam bore a damaged zone at [820, 840] mm, which was simulated by reducing the Young's modulus by 50 percent of their original value within the damaged zone. To avoid the influence from the excitation, an inspection region, $x \in [200, 1200]$ mm, was selected to exclude the vicinity of the excitation point.

The flexural displacement at each FE node (corresponding to the measurement point in a subsequent experiment) in the absence of noise interference, denoted by w_i^{exact}, was obtained using ANSYS®, which was then numerically contaminated

Table 1
Material and geometrical properties of the cantilever beam in FE analysis.

Density ρ [kg/m^3]	2700
Young's modulus E [GPa]	70
Beam length L [mm]	1200
Width b [mm]	10
Thickness h [mm]	10

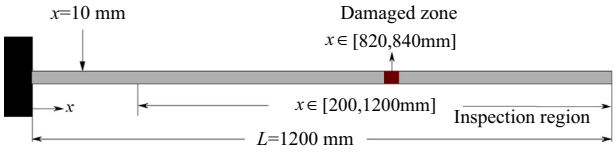

Fig. 4. A cantilever beam bearing a small damaged zone in FE analysis.

with added noise as

$$w_i^{\text{noisy}} = w_i^{\text{exact}} \cdot (1+\varepsilon_i) \cdot e^{j\varphi_i}, \tag{7}$$

where w_i^{noisy} is the noise-corrupted counterpart of w_i^{exact}; ε_i is a Gaussian random real number related to the magnitude of w_i^{exact}; and φ_i is another Gaussian random real number related to the phase of w_i^{exact}. In the succeeding analysis, $\mu(\varepsilon_i)=\mu(\varphi_i)=0$, $\sigma(\varepsilon_i)=1\%$ and $\sigma(\varphi_i)=1^\circ$ (μ and σ signify the mathematical manipulation to calculate the mean and the standard deviations, respectively). The noise of such a level is indistinguishable between w_i^{exact} and w_i^{noisy}.

4.2.2. Identification of damage using "Strong Formulation"

With w_i^{exact} and w_i^{noisy}, the correspondingly constructed DI^{exact} and DI^{noisy}, using the "strong formulation" of the PE approach (Eq. (2c)), are displayed in Fig. 5. DI^{exact}, Fig. 5(a), explicitly and accurately indicates the location of the damaged zone by revealing its two ends. On the contrary, DI^{noisy}, Fig. 5(b), fails to pinpoint the damaged zone, because the added noise, though low in its level, masks the damage-induced changes in the damage index significantly, which can be attributed to the drastic magnification of the noise in the signal during the fourth-order differentiation. Such an observation is in agreement with the analyses made previously.

4.2.3. Identification of damage using CGS-based "Weak Formulation"

w_i^{exact} and w_i^{noisy} were then processed with CGS-based "weak formulation" defined by Eq. (6a). Fig. 6(a) to (h) presents correspondingly constructed $\overline{\text{DI}}_{4-\text{CGS}}^{\text{exact}}$ and $\overline{\text{DI}}_{4-\text{CGS}}^{\text{noisy}}$, using various integration windows (when τ/λ of Ξ equals to 0.27, 0.5, 1 and 1.32, respectively; λ is the vibration wavelength of the beam which is 0.3 m under the current excitation frequency). With a smaller Ξ (Fig. 6(a) and (b)), both $\overline{\text{DI}}_{4-\text{CGS}}^{\text{exact}}$ and $\overline{\text{DI}}_{4-\text{CGS}}^{\text{noisy}}$ show greater similarity, respectively, with DI^{exact} and DI^{noisy} in Fig. 5 which are obtained using the "strong formulation". This implies that the anticipated advantages of the "weak formulation" over "strong formulation" tend to be obscure when the integration interval becomes smaller. On the contrary, with an increase in Ξ, a dual effect can be observed: (i) the detection resolution decreases, as seen in Fig. 6(a), (c), (e) and (g) for $\overline{\text{DI}}_{4-\text{CGS}}^{\text{exact}}$, because of a progressively enlarged Ξ; (ii) the noise immunity of the damage index increases, in Fig. 6(b), (d), (f) and (h) for $\overline{\text{DI}}_{4-\text{CGS}}^{\text{noisy}}$, because of the intensified averaging of measurement noise with more measurement points included in Ξ.

It is therefore crucial to strike a balance between the detection resolution and the noise immunity for the CGS-based damage index through optimizing τ/λ. In Fig. 6, it is obvious that a reasonable compromise can be reached when $\tau/\lambda=1$, – the case in Fig. 6(f), with which the damaged zone can be located with satisfactory resolution using $\overline{\text{DI}}_{4-\text{CGS}}^{\text{noisy}}$. However, to achieve such a compromise is a challenging task, as the adjustment of τ/λ simultaneously changes the number of the measurement points included in Ξ (N in the following), incurring additional influence on the detection accuracy.

To interrogate such an influence from N, τ/λ is kept to be constant (i.e., $\tau/\lambda=1$), and N is reduced gradually from 151 to 38 in this case, giving rise to different detection results obtained using $\overline{\text{DI}}_{4-\text{CGS}}^{\text{exact}}$ and $\overline{\text{DI}}_{4-\text{CGS}}^{\text{noisy}}$, as shown in Fig. 7(a) to (f) ($N=151$ in (a) and (b); $N=76$ in (c) and (d); $N=38$ in (e) and (f)). It can be seen that the distribution of $\overline{\text{DI}}_{4-\text{CGS}}^{\text{exact}}$ basically remains unchanged regardless of N. However, the decrease in N affects the distribution of $\overline{\text{DI}}_{4-\text{CGS}}^{\text{noisy}}$ considerably. These observations reveal that, at a given τ/λ, the noise influence becomes more phenomenal with less measurement points in Ξ, – a possibility to suppress noise along with improved detection accuracy in practical implementations. On the other hand, reduction in N simultaneously increases d_m (the distance between two adjacent measurement points), in turn influencing detection accuracy as well. Further insight into the relationship among different parameters (e.g., τ, d_m, and N) and their influence on detection accuracy is to be given in Section 4.4.

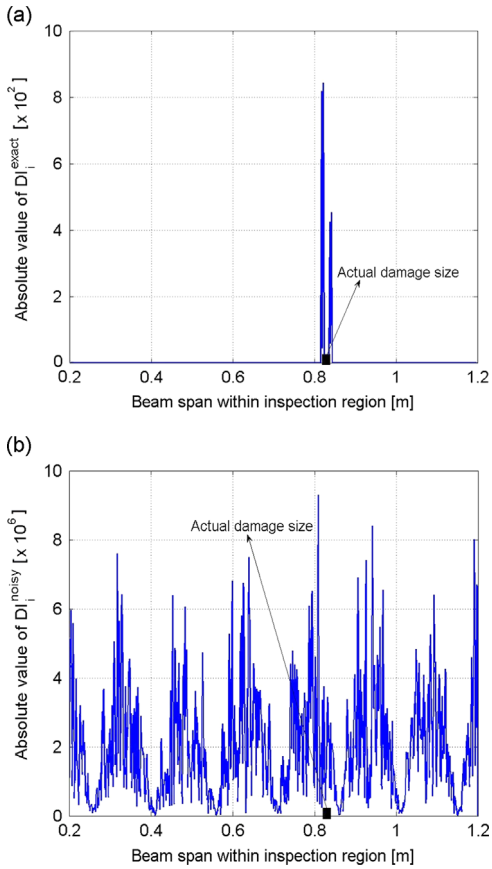

Fig. 5. Constructed DI_i using the "strong formulation" using (a) noise-free and (b) noise-contaminated vibration displacements.

Similarly, different orders of the CGS-based damage indices, $\overline{DI}^{noisy}_{3-CGS}$, $\overline{DI}^{noisy}_{2-CGS}$, $\overline{DI}^{noisy}_{1-CGS}$, and $\overline{DI}^{noisy}_{0-CGS}$, at the above said optimal setting when $\tau/\lambda = 1$ ($N = 151$), were obtained using Eqs. (6b) to (6e), and their distribution is displayed in Fig. 8, highly resembling those results in Fig. 6 in which $\overline{DI}^{noisy}_{4-CGS}$ is concerned. The high similarity among different orders of the "weak formulation", from $\overline{DI}^{noisy}_{4-CGS}$to $\overline{DI}^{noisy}_{0-CGS}$ confirms the mathematical nature of the "weak formulation", as illustrated previously in Section 3.3: $\overline{DI}_k$ of different orders ($k = 0,\ 1,\ 2,\ 3,\ 4$) are in principle identical, provided there are sufficient measurement points within Ξ.

4.3. Experimental validation

4.3.1. Setup

Experimental validation was subsequently conducted, to identify multiple cracks in a cantilever beam (aluminum 6061, Young's modulus: 68.9 GPa, mass density: 2700 kg/m^3, and Poisson's ratio: 0.27) which was fixed-supported on a testing table (NEWPORT® ST-UT2), as sketched in Fig. 9. The defined inspection region, shown in Fig. 9, featured a length of 550 mm, a constant width of 30 mm and a uniform thickness of 8 mm, within which two through-width cracks (1.2 mm × 30 mm × 2 mm for each, i.e., 0.2 percent of the beam-span) were pre-treated at 220 mm and 380 mm from the clamped end of the beam, respectively. Notably, the irregular shape of the beam, i.e., non-constant width near the free end, was intentionally designed, in order to demonstrate the effectiveness of the PE technique and its "weak formulation" in detecting damage in beam components with complex boundary geometries. A harmonic point-force excitation of 2000 Hz was applied on the beam with an electromechanical shaker (B&K®4809), near the free end of the beam, this leading to a λ of 0.18 m approximately. A scanning Doppler laser vibrometer (Polytec®PSV- 400B) was used to measure the out-of-plane flexural deflections at 210 measurement points (with a spacing interval of 2.6 mm), along the central line of the beam within the inspection region. It took circa twenty minutes to finish a single test. During the scanning, the measurement noise may come from a variety of sources, such as the measurement error of the PSV, the non-perfect boundary condition of the cantilever beam, the non-perfect excitation provided by the electro-mechanical shaker, etc.

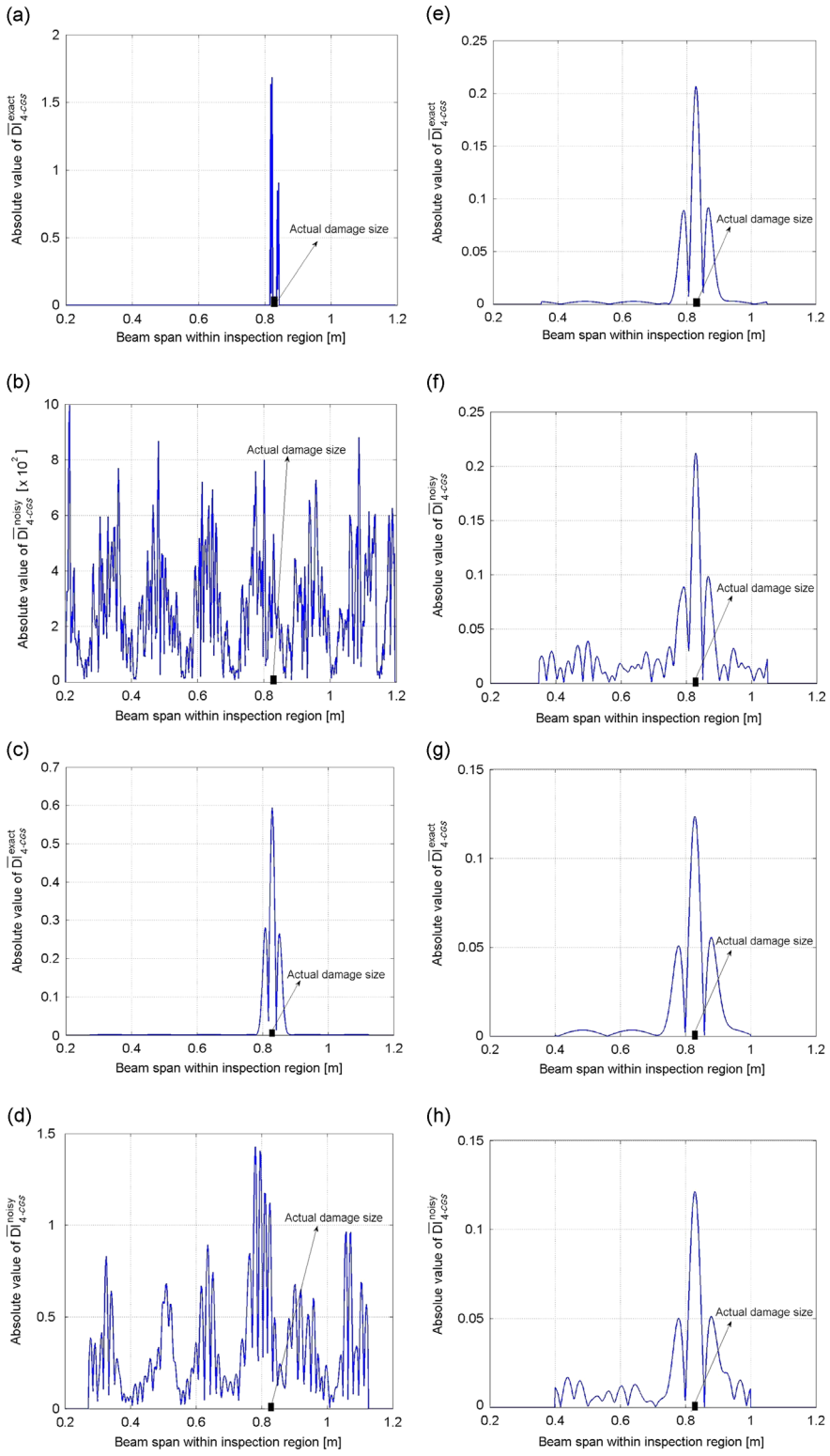

Fig. 6. Distributions of (a) $\overline{DI}^{exact}_{4-CGS}$ when $\tau/\lambda = 0.27$($N = 41$); (b) $\overline{DI}^{noisy}_{4-CGS}$ when $\tau/\lambda = 0.27$($N = 41$); (c) $\overline{DI}^{exact}_{4-CGS}$ when $\tau/\lambda = 0.5$ ($N = 76$); (d) $\overline{DI}^{noisy}_{4-CGS}$ when $\tau/\lambda = 0.5$ ($N = 76$); (e) $\overline{DI}^{exact}_{4-CGS}$ when $\tau/\lambda = 1$ ($N = 151$); (f) $\overline{DI}^{noisy}_{4-CGS}$ when $\tau/\lambda = 1$ ($N = 151$); (g) $\overline{DI}^{exact}_{4-CGS}$ when $\tau/\lambda = 1.32$ ($N = 201$); and (h) $\overline{DI}^{noisy}_{4-CGS}$ when $\tau/\lambda = 1.32$ ($N = 201$).

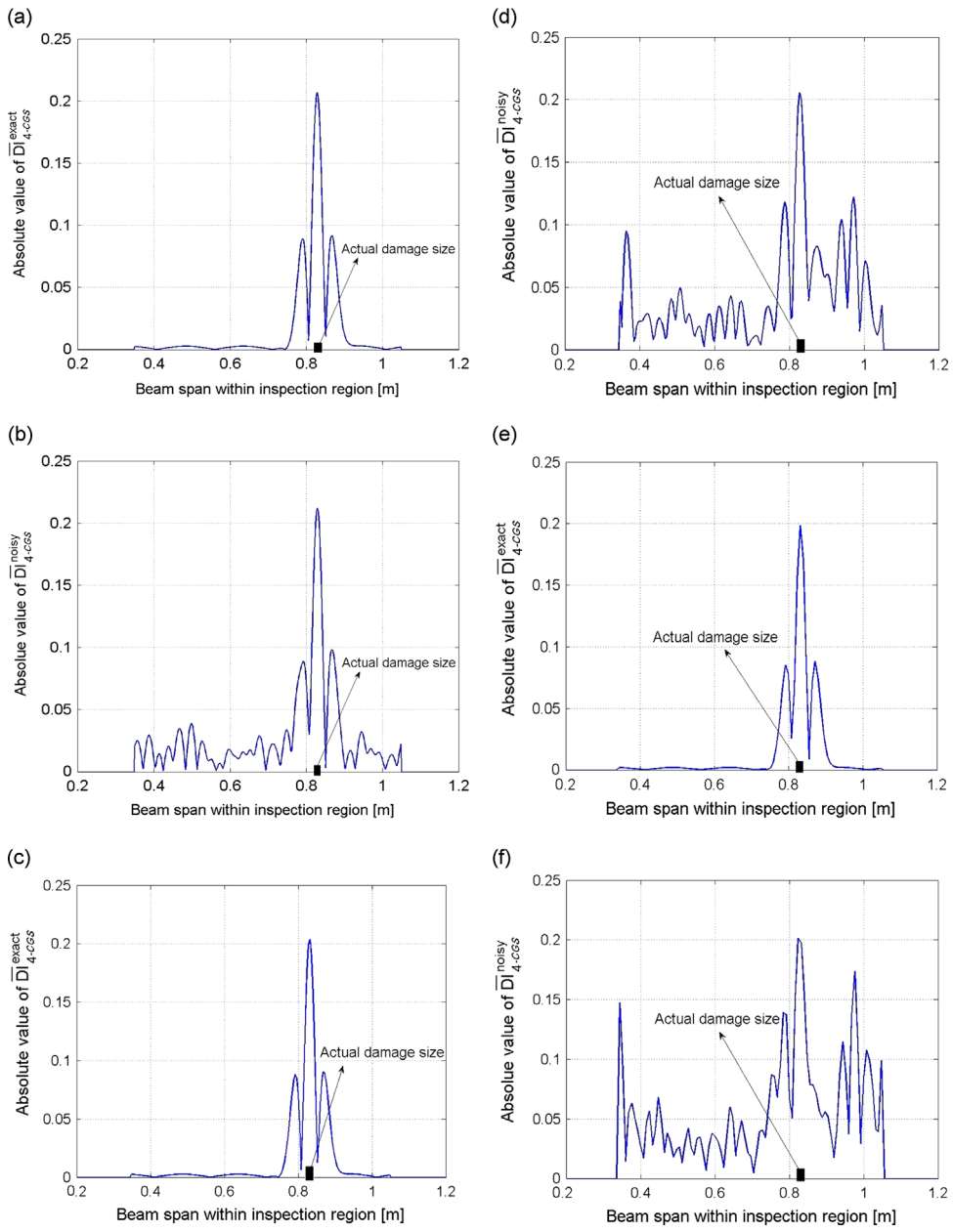

Fig. 7. At $\tau/\lambda = 1$, distributions of (a) $\overline{DI}^{exact}_{4-CGS}$ when $N = 151$; (b) $\overline{DI}^{noisy}_{4-CGS}$ when $N = 151$; (c) $\overline{DI}^{exact}_{4-CGS}$ when $N = 76$; (d) $\overline{DI}^{noisy}_{4-CGS}$ when $N = 76$; (e) $\overline{DI}^{exact}_{4-CGS}$ when $N = 38$; and (f) $\overline{DI}^{noisy}_{4-CGS}$ when $N = 38$.

4.3.2. Results and discussion

As representative results, the absolute values of w_i across the inspection region under the above excitation are shown in Fig. 10(a), along with the damage index constructed using "strong formulation" of the PE approach shown in Fig. 10(b). As anticipated, the "strong formulation"-based damage index fails to delineate any damage, because of the interference from measurement noise. On the contrary, $\overline{DI}_{4-CGS}$ calculated using Eq. (6a) is displayed in Fig. 11 (for several τ/λ values, namely, different Ξ). In Fig. 11(a) (when $\tau/\lambda = 0.14$), the "weak formulation" of the PE approach does not present significantly improved de-noising effect, and the profile of corresponding $\overline{DI}_{4-CGS}$ shows great similarity with that of the index calculated using "strong formulation" shown in Fig. 10(b). When τ/λ is increased to 0.33, improvement of detection accuracy is observed, as shown in Fig. 11(b), whereby the location of one of the two cracks can be identified, more or less, though the other is yet masked by the noise. With an even greater Ξ (when $\tau/\lambda = 0.6$), satisfactory detection accuracy is reached, in Fig. 11(c), in which locations of both cracks are identified precisely. However, progressive enlargement of τ/λ does not lead to further improved detection accuracy, instead a decrease of the resolution is noticed, as seen in Fig. 11(d) where $\tau/\lambda = 0.95$. This is in consistent with the conclusion drawn previously that a balance between the detection resolution and noise

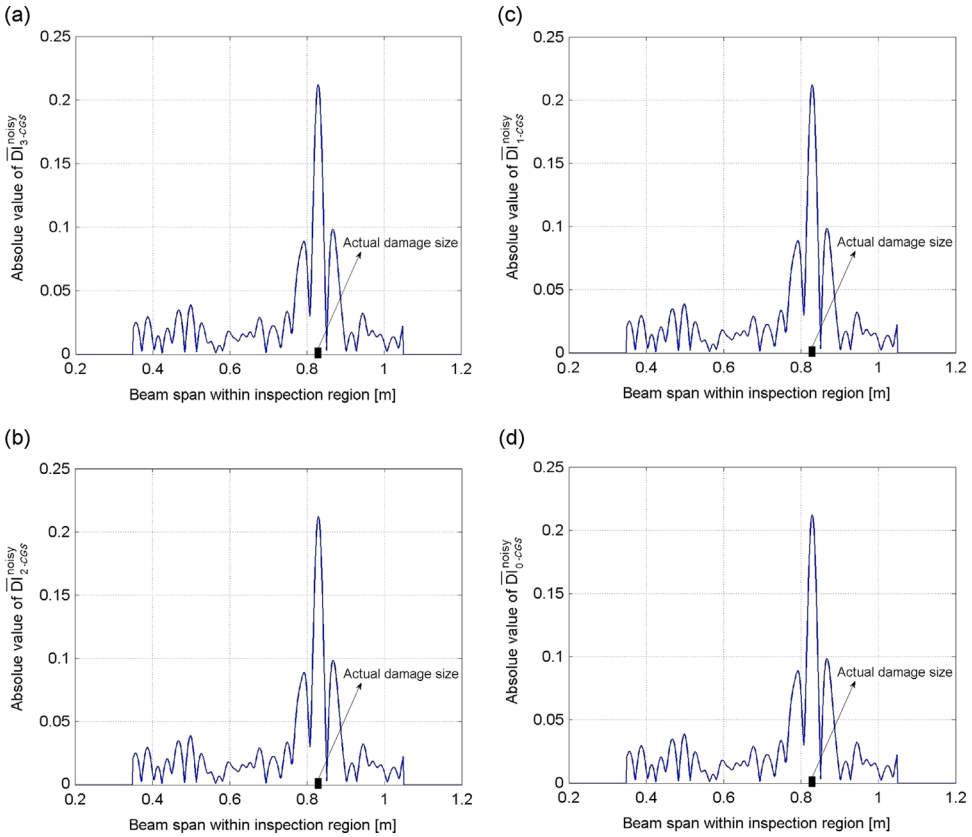

Fig. 8. At $\tau/\lambda = 1$, distributions of (a) $\overline{DI}^{noisy}_{3-CGS}$; (b) $\overline{DI}^{noisy}_{2-CGS}$; (c) $\overline{DI}^{noisy}_{1-CGS}$; and (d) $\overline{DI}^{noisy}_{0-CGS}$.

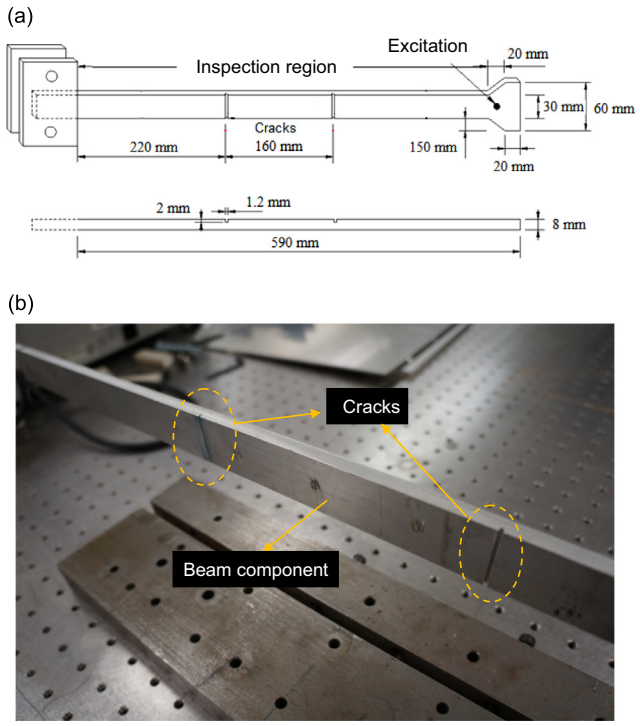

Fig. 9. Experimental validation: (a) schematic of a cantilever beam bearing two cracks and (b) photo of the cracks in the inspection region.

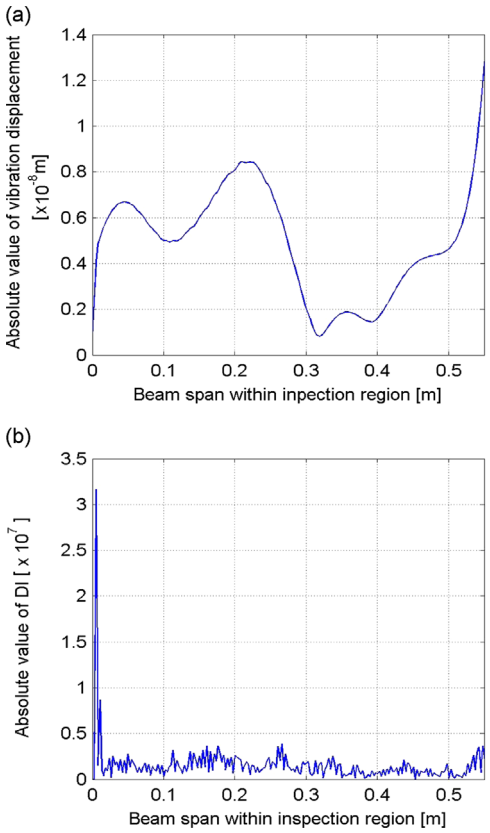

Fig. 10. (a) The vibration displacements of the beam subject to the excitation and (b) the constructed DI_i using the 'strong formulation.'

immunity can be obtained through optimizing τ/λ. In addition, it can be seen that, although the cracks are of the same parameters, the corresponding magnitudes are different as presented in Fig. 11(c). This can be attributed to the fact that the magnitudes of the damage indices of the PE technique vary in accordance with the variation of internal bending moments along the beam [1]. Thus the differences in the magnitude of damage indices are mainly attributed to the differences of bending moments at the two crack locations.

The influence of measurement points included in Ξ (viz., N) on the detection accuracy was then gauged by fixing τ/λ to be 0.6. It is reasonable to see from Fig. 12(a) to (d) that the detection accuracy declines progressively as N decreases. In particular, in Fig. 12(c) (when $N=12$), a pseudo peak of $\overline{\mathrm{DI}}_{4-\mathrm{CGS}}$ (indicating pseudo damage) is observed in the intact region of the beam, and in Fig. 12(d) (when $N=6$), the $\overline{\mathrm{DI}}_{4-\mathrm{CGS}}$ becomes indistinguishable to reveal the position of either of the two cracks, because of insufficient measurement points included Ξ.

4.4. Estimate of noise effect

As commented in Section 3, the effect of measurement noise in the "weak formulation" can be transferred between the "integration part" and the "boundary part", at different orders of the damage index. One can thus make use of such a trait, to facilitate the selection of measurement parameters and experimental configurations with reduced noise effect.

In this backdrop, the "weak formulation" provides a means to estimate the noise effect on the detection accuracy. Mathematically, the integral of any function, say $f(x)$, within an integration interval between a and b can be expressed, according to the principle of Riemann integral [21], as

$$\int_a^b f(x)\mathrm{d}x = \lim_{n\to\infty} \sum_{k=1}^{n} f(x_k^*)\Delta x_k, \tag{8}$$

where x_k^* is an arbitrary point in the sub-interval Δx_k. Provided the measurement density is sufficiently large (viz., there are sufficient measurement points to depict the profile of $w(x)$ accurately), $\overline{\mathrm{DI}}_{0-\mathrm{CGS}}$ defined by Eq. (6e), without and with noise influence, can be approximated, respectively, as

$$\overline{\mathrm{DI}}_{0-\mathrm{CGS}}^{\mathrm{exact}} = d_m \cdot \sum_{r=1}^{N} \Gamma_r \cdot w_r^{\mathrm{exact}}, \tag{9a}$$

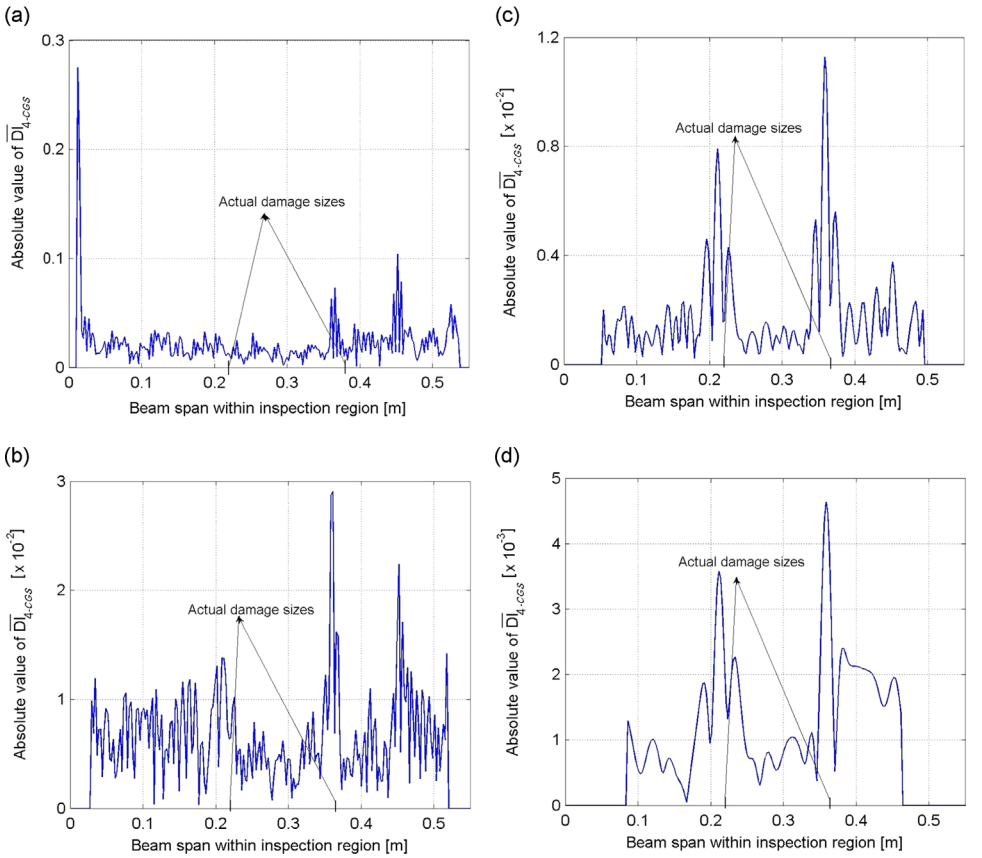

Fig. 11. Distributions of $\overline{\mathrm{DI}}_{4-\mathrm{CGS}}$ when (a) $\tau/\lambda=0.14$ ($N=11$); (b) $\tau/\lambda=0.33$ ($N=25$); (c) $\tau/\lambda=0.6$ ($N=45$); and (d) $\tau/\lambda=0.95$ ($N=71$).

$$\overline{\mathrm{DI}}_{0-\mathrm{CGS}}^{\mathrm{noisy}}=d_m\cdot\sum_{r=1}^{N}\Gamma_r\cdot w_r^{\mathrm{noisy}}, \tag{9b}$$

where

$$\Gamma_r=\frac{EI}{d_m^4}(\eta_{r-2}-4\eta_{r-1}+\eta_r-4\eta_{r+1}+6\eta_{r+2})-\rho S\omega^2\eta_r. \tag{9c}$$

In the above, r is a sequence number of the measurement point locally defined in Ξ. The high-order derivative of $\eta(x)$ in Eq. (6e) can be calculated using a finite difference scheme defined by Eq. (9c). Note that Γ_r in Eq. (9a) and (9b) is free of noise interference. In Eq. (9b), assuming w_r^{noisy} can be expressed in a simplified form (similar to Eq. (7)), as

$$w_r^{\mathrm{noisy}}=w_r^{\mathrm{exact}}\cdot(1+\theta_r), \tag{10}$$

where θ_r is a Gaussian random number, with the mean and standard deviation being $\mu(\theta_r)$ ($\mu(\theta_r)=0$) and $\sigma(\theta_r)$, respectively. θ_r can be either a real number related to the magnitude of w_r^{exact}, or a complex number related to both the magnitude and phase of w_r^{exact}. Then Eq. (9b) can be expanded to

$$\begin{aligned}\overline{\mathrm{DI}}_{0-\mathrm{CGS}}^{\mathrm{noisy}}&=d_m\cdot\sum_{r=1}^{N}\Gamma_r\cdot w_r^{\mathrm{exact}}\cdot(1+\theta_r)\\&=d_m\cdot\sum_{r=1}^{N}\Gamma_r\cdot w_r^{\mathrm{exact}}+d_m\cdot\sum_{r=1}^{N}\Gamma_r\cdot w_r^{\mathrm{exact}}\cdot\theta_r=\overline{\mathrm{DI}}_{0-\mathrm{CGS}}^{\mathrm{exact}}+\Theta,\end{aligned} \tag{11a}$$

where

$$\Theta=d_m\cdot\sum_{r=1}^{N}\Gamma_r\cdot w_r^{\mathrm{exact}}\cdot\theta_r. \tag{11b}$$

Thus, the noise influence on $\overline{\mathrm{DI}}_{0-\mathrm{CGS}}^{\mathrm{exact}}$, all included in Θ, is now isolated. It is important to note that in practical measurement, θ_r is a random variable associated with rth measurement point. According to the theory of probability and statistics [22], Θ is also an independent random variable subject to individual integration interval, conforming to Gaussian distribution, with its

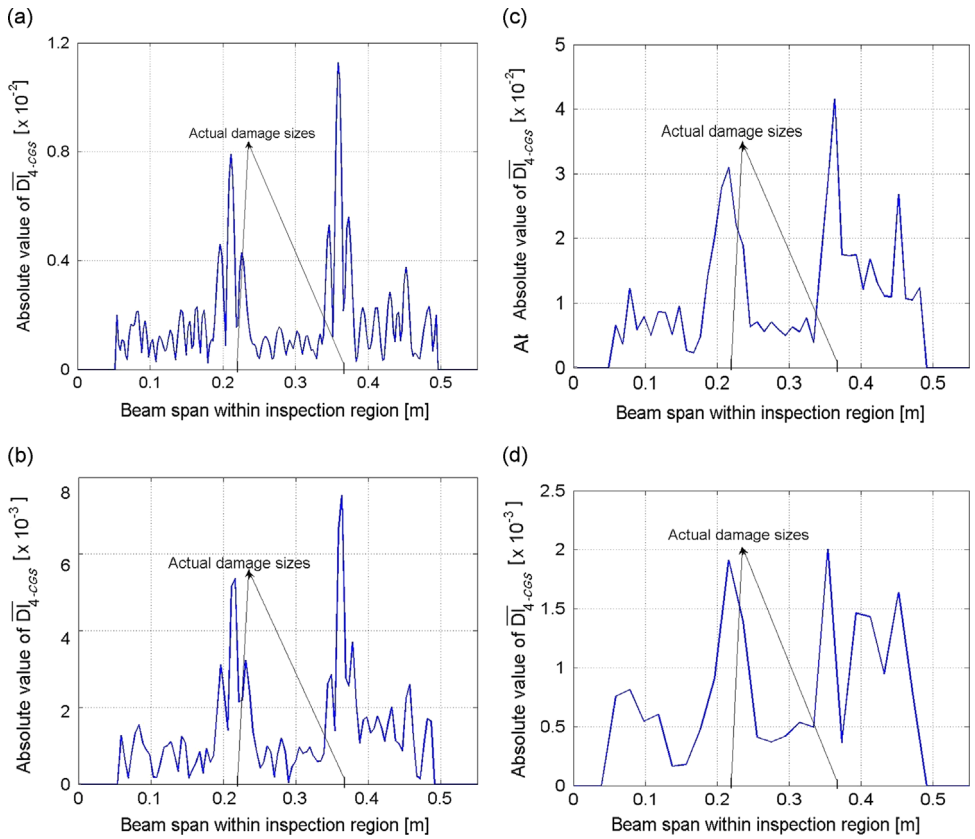

Fig. 12. At $\tau/\lambda = 0.6$, distributions of $\overline{DI}_{4-CGS}$ when (a) $N = 45$; (b) $N = 23$; (c) $N = 12$; and (d) $N = 6$.

mean and standard deviation being

$$\mu(\Theta) = 0, \tag{12a}$$

and

$$\sigma(\Theta) = d_m \cdot \sqrt{\sum_{k=1}^{N} \left(\Gamma_r \cdot w_r^{\text{exact}}\right)^2} \cdot \sigma(\theta_r). \tag{12b}$$

Therefore, the level of noise effect included in $\overline{DI}_{0-CGS}^{\text{noisy}}$ can be estimated quantitatively in terms of $\sigma(\Theta)$, which can also be used to estimate the noise effect in different orders of the "weak formulation" from $\overline{DI}_{1-CGS}^{\text{noisy}}$ to $\overline{DI}_{4-CGS}^{\text{noisy}}$, as all the expanded expressions are mathematically identical. In Eq. (12b), $\sigma(\Theta)$ is substantially determined by several parameters, including (i) d_m, associated with measurement density; (ii) τ, related to the formality of selected $\eta(x)$ and the position of Ξ (serving as a scanning window along inspection region); (iii) N, associated with both the measurement density and the selected τ; and (iv) $\sigma(\theta_k)$, signifying the initial level of measurement noise included in vibration displacement.

As stated in Section 4.2.3, at a given τ/λ, a smaller N corresponds to a greater d_m. Assuming the summation in Eq. 9(a) is a constant regardless of the change in the measurement density, the value of $\sum_{k=1}^{N}\left(\Gamma_r \cdot w_r^{\text{exact}}\right)^2$ is inversely proportional to d_m. However, because of the square root of $\sum_{k=1}^{N}\left(\Gamma_r \cdot w_r^{\text{exact}}\right)^2$ involved in Eq. (12b), d_m actually plays a dominant role in determining the magnitude of $\sigma(\Theta)$. Thus the increase of noise levels along with the decrease of N, as seen in Figs. 7 and 12, can be attributed to the enlargement of d_m.

Reaching this point, it is pertinent to note that the key parameters of the "weak formulation", which essentially impacts on the detection accuracy and the noise immunity, have been expressed explicitly, and linked quantitatively to the noise influence using Eq. (12). Based on these conclusions, measurement parameters can be selected appropriately and adjusted optimally, so as to minimize the noise effect on the detection accuracy. Eq. (12b) is particularly suitable to be used in numerical study as w_r^{exact} can be obtained directly, and in experimental conditions, the overall trend of the noise level can also be calculated by approximating w_r^{exact} through a curve-fitting algorithm based on measured data. It should also be emphasized that in order to improve the accuracy of numerical integration, advanced algorithms other than the above Riemann integral can also be used, though the philosophy of noise estimate remains the same. Moreover, the above means of noise effect estimate is not only applicable to the "weak formulation" of the PE approach, but also to other methods in

conjunction with the use of high-order derivatives of vibration signals such as mode shape curvature [23–26], and other signal processing techniques relying on weighted integration for instance wavelet analysis [27–30].

5. Concluding remarks

A retrofitted modality of the previous PE approach (called "strong formulation") was developed by introducing the weighted integration, which was contrastively termed as "weak formulation". Sharing the same rationale (by gauging damage-induced perturbation to the local dynamic equilibrium of a structural component), all the merits of the "strong formulation" of the PE approach are inherited by the "weak formulation", but the latter exhibits improved capacity in tolerating measurement noise and uncertainties compared with the former. A series of coherent variants of the "weak formulation" was established, offering a diversity of detection strategies through selecting measurement parameters and configurations, and endowing the PE approach with flexibility in experimental manipulability. As an application of the "weak formulation", a continuous gauss smoothing (CGS)-based damage detection scheme was developed, and validated numerically and experimentally by localizing multiple cracks in a beam-like structure, showing satisfactory detection accuracy and improved noise immunity. It has been shown that an optimal selection of the scanning window (i.e., τ/λ) is critical to influence the detection accuracy and the robustness of the approach when measurement noise is not to be ignored. A compromise between the detection resolution and the noise immunity of the CGS-based damage index could be reached by optimizing τ/λ. In addition, it was found that subject to a given τ/λ, the noise influence increases with a decrease in N, the number of measurement points within the integration interval. These all together are conducive to enhance the noise immunity of the approach when implemented under noisy measurement conditions. In addition, $\overline{\mathrm{DI}}_{0-\mathrm{CGS}}$ can be made use of to explicitly quantify the relationship between the measurement density (d_m and N), width of integration ($\sigma(\theta_k)$) and the level of noise influence ($\sigma(\theta_r)$), facilitating selection of measurement parameters and experimental configurations so as to reduce the noise effect.

Acknowledgments

This project is supported by the National Natural Science Foundation of China (Grant nos. 51375414 and 11272272). This project is also supported by the Hong Kong Research Grants Council via General Research Fund (GRF) (Nos. 15214414 and 523313).

References

[1] H. Xu, L. Cheng, Z. Su, J.L. Guyader, Identification of damage in structural components based on locally perturbed dynamic equilibrium, *Journal of Sound and Vibration* 330 (2011) 5963–5981.
[2] M. Cao, L. Cheng, Z. Su, H. Xu, A multi-scale pseudo-force model in wavelet domain for identification of damage in structural components, *Mechanical Systems and Signal Processing* 28 (2012) 638–659.
[3] H. Xu, L. Cheng, Z. Su, J.L. Guyader, Damage visualization based on local dynamic perturbation: theory and application to characterization of multi-damage in a plane structure, *Journal of Sound and Vibration* 332 (2013) 3438–3462.
[4] H. Xu, L. Cheng, Z. Su, J.L. Guyader, P. Hamelin, Reconstructing interfacial force distribution for identification of multi-debonding in steel-reinforced concrete structures using noncontact laser vibrometry, *Structural Health Monitoring* 12 (2013) 507–521.
[5] H. Sohn, C.R. Farrar, F.M. Hemez, D.D. Shunk, D.W. Stinemates, B.R. Nadler, J.J. Czarnecki, *A Review of Structural Health Monitoring Literature: 1996 – 2001, Report LA-13976-MS*, Los Alamos National Laboratory, 2003.
[6] W. Fan, P. Qiao, Vibration-based damage identification methods: a review and comparative study, *Structural Health Monitoring* 10 (2011) 83–111.
[7] Y.S. Lee, M.J. Chung, A Study on crack detection using eigen-frequency test data, *Computers & Structures* 77 (2000) 327–342.
[8] X. Wang, N. Hu, H. Fukunaga, Z.H. Yao, Structural damage identification using static test data and changes in frequencies, *Engineering Structures* 23 (2001) 610–621.
[9] N. Hu, X. Wang, H. Fukunaga, Z.H. Yao, H.X. Zhang, Z.S. Wu, Damage assessment of structures using modal test data, *International Journal of Solids and Structures* 38 (2001) 3111–3126.
[10] J.T. Kim, Y.S. Ryu, H.M. Cho, N. Stubbs, Damage identification in beam-type structures: frequency-based method vs. mode-shape-based method, *Engineering Structures* 25 (2003) 57–67.
[11] Z. Ismail, H.A. Razak, A.G.A. Rahman, Determination of damage location in rc beams using mode shape derivatives, *Engineering Structures* 28 (2006) 1566–1573.
[12] A. Raghavan, C.E.S. Cesnik, Review of guided-wave structural health monitoring, *The Shock and Vibration Digest* 39 (2007) 91–114.
[13] Z. Su, L. Ye, Y. Lu, Guided Lamb waves for identification of damage in composite structures: a review, *Journal of Sound and Vibration* 295 (2006) 753–780.
[14] W. Ostachowicz, P. Kudela, P. Malinowski, T. Wandowski, Damage localisation in plate-like structures based on PZT sensors, *Mechanical Systems and Signal Processing* 23 (2009) 1805–1829.
[15] J.-B. Ihn, F.-K. Chang, Pitch-catch active sensing methods in structural health monitoring for aircraft structures, *Structural Health Monitoring* 7 (2008) 5–19.
[16] K. Worden, S.G. Pierce, G. Manson, W.R. Philp, W.J. Staszewski, B. Culshaw, Detection of defects in composite plates using lamb waves and novelty detection, *International Journal of Systems Science* 31 (2000) 1397–1409.
[17] X. Zhao, H. Gao, G. Zhang, B. Ayhan, F. Yan, C. Kwan, J.L. Rose, Active health monitoring of an aircraft wing with embedded piezoelectric sensor/actuator network: I. defect detection, localization and growth monitoring, *Smart Materials and Structures* 16 (2007) 1208–1217.
[18] P. Fromme, P.D. Wilcox, M.J.S. Lowe, P. Cawley, On the development and testing of a guided ultrasonic wave array for structural integrity monitoring, *IEEE Transactions on Ultrasonics, Ferroelectrics and Frequency* 53 (2006) 777–785.
[19] J.E. Michaels, T.E. Michaels, Guided wave signal processing and image fusion for in situ damage localization in plates, *Wave Motion* 44 (2007) 482–492.
[20] S.M. Ross, *Introduction to Probability Models*, Academic Press, New York, 1975.
[21] P.J. Davis, P. Rabinowitz, *Methods of Numerical Integration*, Academic Press, New York, 1975.

[22] S.M. Ross, *Introduction to Probability and Statistics for Engineers and Scientists*, Academic Press, New York, 2004.
[23] A.K. Pandey, M. Biswas, M.M. Samman, Damage detection from changes in curvature mode shapes, *Journal of Sound Vibration* 145 (1991) 321–332.
[24] P. Qiao, K. Lu, W. Lestari, J. Wang, Curvature mode shape-based damage detection in composite laminated plates, *Composite Structure* 80 (2007) 409–428.
[25] A. Tomaszewska, Influence of statistical errors on damage detection based on structural flexibility and mode shape curvature, *Computers and Structures* 88 (2010) 154–164.
[26] E. Sazonov, P. Klikhachorn, Optimal spatial sampling interval for damage detection by curvature or strain energy mode shapes, *Journal of Sound and Vibration* 285 (2005) 783–801.
[27] Z. Hou, M. Noori, R. Amand, Wavelet-based approach for structural damage detection, *Journal of Engineering Mechanics* 126 (2000) 677–683.
[28] Z. Sun, C.C. Chang, Structural damage assessment based on wavelet packet transform, *Journal of Structural Engineering* 128 (2002) 1354–1361.
[29] M. Rucka, K. Wilde, Application of continuous wavelet transform in vibration based damage detection method for beams and plates, *Journal of Sound and Vibration* 297 (2006) 536–550.
[30] S.C. Zhong, S.O. Oyadiji, Crack detection in simply supported beams without baseline modal parameters by stationary wavelet transform, *Mechanical Systems and Signal Processing* 21 (2007) 1853–1884.